FMRP REGULATES NEURONAL MIGRATION VIA MAP1B

S. Messaoudi, J. Stoufflet, C. Fouquet, M. Doulazmi, A. Allam, T. Paillard, A. Trembleau, I. Caillé

ABSTRACT

The Fragile X Syndrome (FXS) is the most common form of inherited intellectual disability, and the first monogenic cause of Autism Spectrum Disorder. FXS is caused by the absence of the RNA-binding protein FMRP (Fragile X Messenger Ribonucleoprotein).

Neuronal migration is an essential step of brain development allowing displacement of neurons from their germinal niches to their final integration site.

The precise role of FMRP in neuronal migration remains mostly unexplored. We studied the consequences of FMRP absence on migration, using the postnatal Rostral Migratory Stream (RMS) as an experimental system.

In *Fmr1-null* RMS, neurons exhibit a slowed-down migration and an impaired trajectory, associated with defects of their centrosomal movement. Through RNA-interference-induced knockdown of *Fmr1*, we show that these migratory defects are cell-autonomous. Finally, we show that the FMRP mRNA target involved in these defects is MAP1B (Microtubule-Associated Protein 1B), whose knockdown rescues most migratory defects.

Our results thus unveil a new neurodevelopmental role of FMRP, as a crucial actor of neuronal migration, potentially important for the understanding of FXS pathophysiology.

INTRODUCTION

The Fragile X syndrome (FXS) is the most common cause of inherited intellectual disability and a leading cause of autism spectrum disorder. FXS is due to the silencing of the gene *FMR1* and loss of the encoded protein, FMRP (Fragile X Messenger Ribonucleoprotein) (Davis & Broadie, 2017). FMRP is an ubiquitous RNA-binding protein, with high level of expression in the central nervous system (Gholizadeh *et al*, 2015). It is a general regulator of RNA metabolism and especially of mRNA local translation in neurons (Banerjee *et al*, 2018). Its cognate mRNA targets are numerous

and diverse, including mRNAs encoding proteins involved in neuronal plasticity like CamKIIα (Calcium Calmodulin-dependent Kinase II) and cytoskeletal proteins like MAP1B (Microtubule-Associated Protein 1B) (Ascano *et al*, 2012)(Brown *et al*, 2001)(Darnell *et al*, 2001)(Maurin *et al*, 2018). *Fmr1*-null mice are the murine model of FXS and have allowed characterization of neurodevelopmental and plasticity defects consecutive to the absence of FMRP. We previously showed the essential role of FMRP in the differentiation and learning-induced structural plasticity of adult-generated olfactory bulb interneurons (Scotto-Lomassese *et al*, 2011)(Daroles *et al*, 2016).

Neuronal migration is a crucial step for the establishment of neuronal circuitry. It allows the displacement of neurons from their site of birth to their final destination of differentiation. Migration defects lead to severe brain pathologies like lissencephaly and cortical heterotopia and might be involved in psychiatric disorders (Romero *et al*, 2018). Interestingly, migration in the human infant brain appears to be even more extended than anticipated from the rodent data (Sanai *et al*, 2011)(Paredes *et al*, 2016). In addition, periventricular heterotopia was described in two FXS patients, suggesting a possible role for FMRP in migration (Moro *et al*, 2006). However, the question of potential migration defects in FXS remains mostly unexplored. In *Fmr1*-null mice, radially migrating embryonic glutamatergic cortical neurons display a defect in the multipolar to bipolar transition (La Fata *et al*, 2014), a critical change of polarity taking place before the initiation of the movement. Additionally, FMRP overexpression of knockdown leads to misplacement of cortical glutamatergic neurons, also suggesting its role in radial embryonic migration (Wu *et al*, 2019). However, to our knowledge, tangential neuronal migration in the absence of FMRP has not been studied so far and, more generally, the dynamics of mutated *Fmr1* neurons have never been analyzed in detail.

The Rostral Migratory Stream (RMS) is the main avenue for migrating neurons in the postnatal and adult mouse brain (Lois *et al*, 1996). A massive number of neuroblasts are constantly produced in the ventricular/subventricular zone (V/SVZ) and migrate over a long distance along the RMS to the olfactory bulb (OB) (Lim & Alvarez-Buylla, 2016). They display a cyclic saltatory mode of migration, in which the nucleus and centrosome move forward in a “two-stroke” cycle. The centrosome moves

first within a swelling in the extending leading process and the nucleus follows subsequently (Bellion *et al*, 2005).

Here, using the postnatal RMS as a migration model as in (Stoufflet *et al*, 2020), we show entirely novel migratory defects induced by the absence of FMRP. Migrating neurons display a slowed-down and more erratic migration in *Fmr1*-null mice, accompanied by defects in their centrosome movement. These defects are cell-autonomous, since recapitulated by RNA-interference-induced *Fmr1* knockdown (KD). Given the known role of MAP1B (Microtubule Associated Protein 1B) in neuronal migration, we suspected that it might be the FMRP mRNA target involved in the observed defects. MAP1B level is indeed increased in the mutated RMS and its downregulation rescues most migration defects, showing that FMRP regulates neuronal migration through MAP1B.

MATERIAL AND METHODS

Mouse lines

Mice were housed in a 12 hours light/dark cycle, in cages containing one or two females and one male. The postnatal mice were housed in their parents' cage. Animal care was conducted in accordance with standard ethical guidelines [National Institutes of Health (NIH) publication no. 85-23, revised 1985 and European Committee Guidelines on the Care and Use of Laboratory Animals 86/609/EEC]. The experiments were approved by the local ethics committee (Comité d'Ethique en Expérimentation Animale Charles Darwin C2EA-05 and the French Ministère de l'Education Nationale, de l'Enseignement Supérieur et de la Recherche APAFIS#13624-2018021915046521_v5). We strictly performed this approved procedure. The mice used were in a C57BL6-J background. *Fmr1-null* mice were genotyped according to the original protocol (Fmr1 knockout mice: a model to study fragile X mental retardation. The Dutch-Belgian Fragile X Consortium, 1994).

MiRNA production

Silencing of *Fmr1* and *Map1b* has been performed using BLOCK-iT Pol II miR RNAi Expression Vector Kits (Invitrogen) and the RNAi Designer (Invitrogen). The sequences of the single-stranded oligos are:
Fmr1 Top: TGCTGTACAAATGCCTTGTAGAAAGCGTTTTGGCCAACTGACTGACGCTTTCTAAGGCATTTGTA,
Fmr1 Bottom: CCTGTACAAATGCCTTAGAAAGCGTCAGTCAGTGGCCAAAACGCTTTCTACAAGGCATTTGTAC,
Map1b Top:

TGCTGTGTTGATGAAGTCTTGGAGATGTTTTGGCCACTGACTGACATCTCCAAC
TTCATCAACA,
Map1b Bottom:
CCTGTGTTGATGAAGTTGGAGATGTCAGTCAGTGGCCAAAACATCTCCAAGACT
TCATCAACAC.
The double-stranded oligos were inserted in a pcDNA 6.2-GW/EmGFP-miR. The resulting constructions were sequenced before use.

Postnatal electroporation

Postnatal injection and electroporation were performed at postnatal day 2 (P2). Postnatal mice were anesthetized by hypothermia. Pseudo-stereotaxic injection [from lambda medial-lateral (M/L): 0,9; anterior-posterior (A/P): 1,1; dorsal-ventral (D/V): 2] using a glass micropipette (Drummond Scientific Company, Wiretrol I, 5-000-1050) was performed, and 2ul of plasmid (between 5 and 8 μg/ml) was injected. Animals were subjected to 5 pulses of 99.9V during 50ms separated by 950ms using the CUY21 SC Electroporator and 10-mm tweezer electrodes (Harvard Apparatus, Tweezertrode, 10mm, 45-0119). The animals were placed on 37°C plates to restore their body temperature before returning in their parents' cage. Animals were considered as fully restored when moving naturally and their skin color returned to pink.

Postnatal acute brain slices

Brain slices of mice aged from P6 to P10 were prepared as previously described in (Stoufflet *et al*, 2020). Pups were sacrificed by decapitation and the brain was removed from the skull. Sagittal brain sections (250 μm) were cut with a VT1200S microtome (Leica). Slices were prepared in an ice-cold cutting solution of the following composition: 125 mM NaCl, 0.4 mM $CaCl_2$, 1 mM $MgCl_2$, 1.25 mM NaH_2PO_4, 26 mM $NaHCO_3$, 5 mM sodium pyruvate, 20 mM glucose and 1 mM kynurenic acid, saturated with 5% CO_2 and 95% O_2. Slices were incubated in this solution for 30 minutes at room temperature and then placed in recording solution (identical to the cutting solution, except that the $CaCl_2$ concentration is 2 mM and kynurenic acid is absent) for at least 30 minutes at 32°C before image acquisition.

Time-lapse video microscopy of postnatal slices

To analyze neuronal migration and centrosome dynamics, images were obtained with an inverted SP5D confocal microscope (Leica) using a 40x/1.25-numerical aperture (N.A.) objective with 1.5 optical zoom or an upright SP5 MPII two-photon microscope (Leica) using a 25x/0.95-N.A. objective with 1.86 optical zoom. Images were acquired every 3 minutes for 2 to 3 hours. The temperature in the microscope chamber was maintained at 32°C during imaging and brain slices were continuously perfused with heated recording solution (see above) saturated with 5% CO_2 and 95% O_2.

Analyses of neuronal migration and centrosome movement

Analyses were performed using ImageJ (NIH Image; National Institutes of Health, Bethesda, MD) software and MTrackJ plugin (Meijering, Dzyubachyk, et Smal 2012). The nucleus and the centrosome (when centrin-RFP was co-injected) were tracked

manually on each time frame during the whole movie. We considered a NK as a movement superior to 6 μm between two consecutive time points (3 minutes-interval). For cell migration, calculation of speed, percentage of pausing time, sinuosity, directionality, NK distance and frequency was performed using the x,y,t coordinates of the nucleus of each cell. Cells tracked for less than 30 minutes and cells that did not perform any NK during the whole tracking were excluded. A CK was defined as a forward movement superior to 2 μm followed by a backward movement superior to 2 μm. For centrosome movement, calculation of CK speed, frequency and efficiency was performed using the x,y,t coordinates of the centrosome of each cell and the x,y,t coordinates of each corresponding nucleus.

Immunohistochemistry

P7 to P10 mice were lethally anesthetized using Euthasol. Intracardiac perfusion with 4% paraformaldehyde was performed. The brain was post-fixed overnight in 4% paraformaldehyde and then rinsed three times with phosphate-buffered saline (PBS) 1x (Gibco, 1400-067). 50 μm sagittal sections were made with VT1200S microtome (Leica). Slices were placed 1 hour in a saturation solution (10% fetal bovine serum; 0.5% Triton X-100 in PBS). Primary antibodies used in this study are: GFP (Aves; GFP-1020; 1/1000), FMRP (Developmental Studies Hybridoma Bank; 2F5-1; 1/200), MAP1B (Santa Cruz Biotechnology; sc-365668; 1/300). The antibodies were diluted in saturation solution. Slices were incubated for 48 to 72 hours at 4°C under agitation with the antibodies and then rinsed three times with PBS 1x. Secondary antibodies used are: anti-chicken immunoglobulin Y (IgY) Alexa Fluor 488 (1/1000; Jackson ImmunoResearch; 703-545-155) against anti-GFP, anti-mouse immunoglobulin G2b (IgG2b) Alexa Fluor 555 (1/2000; Jackson ImmunoResearch; 703-545-155) against anti-FMRP and anti-MAP1B. The antibodies were diluted in saturation solution. Slices were incubated with secondary antibodies for 1 hour at room temperature under agitation, protected from light. After rinsing three times with PBS 1x, slices were counter-colored with Hoechst and mounted in Mowiol.

Tissue collection and Western blotting

RMS were manually micro-dissected from 5 to 6 postnatal mouse brains and pooled in a PBS 1x (0.5% glucose) solution. After centrifugation, protein extraction was performed on the tissue pellet. Samples were homogenized in a lysis buffer with the following composition: 25 mM Tris HCl pH 7.5, 150 mM NaCl, 1% NP40, 0.5% NaDeoxycholate, 1 mM EDTA, 5% glycerol, 1X EDTA-free protease inhibitor cocktail (Sigma, 4693132001). After centrifugation, samples were loaded and run in NuPAGE 3-8% Tris-Acetate Gel (Invitrogen, EA0378BOX) at 120V for 15 minutes then 180V for 40 minutes. Transfer to nitrocellulose Immobilon-PVDF-P membrane (Millipore, IPVH00010) was performed at 40V overnight at 4°C. The membrane was then saturated for 1 hour in TBSt containing 5% powder milk. Primary antibodies used are: MAP1B (Santa Cruz Biotechnology, sc-365668, 1/100), Vinculin (Cell Signaling Technology, 13901S, 1/1000). The antibodies were diluted in TBSt containing 5% powder milk. Secondary antibodies used are: ECL anti-mouse immunoglobulin G (IgG) horseradish peroxidase linked whole antibody (1/10 000; Fisher Scientific; NXA931V) for anti-MAP1B, Peroxidase-conjuguated AffiniPure F(ab')2 Fragment Donkey Anti-Rabbit IgG (H+L) (1/5 000; Jackson ImmunoResearch; 711-036-152) for anti-Vinculin. The antibodies were diluted in TBSt containing 5% powder milk. Labeling was

visualized using Pierce ECL Western Blotting Substrate (Thermo Scientific; 32209) and luminescent image analyzer LAS-3000.

Statistics

All manipulations and statistical analyses were implemented with R (4.2.1, R Foundation for Statistical Computing, Vienna, Austria). Normality in the variable distributions was assessed by the Shapiro-Wilk test. Furthermore, the Levene test was performed to probe homogeneity of variances across groups. Variables that failed the Shapiro-Wilk or the Levene test were analyzed with non-parametric statistics using the one-way Kruskal-Wallis analysis of variance on ranks followed by Nemenyi test post hoc and Mann-Whitney rank sum tests for pairwise multiple comparisons. Variables that passed the normality test were analyzed by means of one-way ANOVA followed by Tukey post hoc test for multiple comparisons or by Student's *t* test for comparing two groups. Categorical variables were compared using Pearson's c^2 test or Fisher's exact test. A *p*- value of <0.05 was used as a cutoff for statistical significance. Results are presented as the means ± SEM. The statistical tests are described in each figure legend.

RESULTS

FMRP is expressed in migrating neurons of the postnatal RMS

We use the postnatal RMS (Rostral Migratory Stream) as a model system to study migration. In this stream, neurons are born in the ventricular-subventricular niche and follow a tangential path toward the olfactory bulb (Fig. 1.A). During their progression, neurons display a stereotypical bipolar morphology with a long leading process and a short trailing one. They perform a "two-stroke" cycle. Initially, they extend their leading process and their centrosome moves forward within a swelling at a distance from the nucleus (centrokinesis (CK)). This is followed by a subsequent movement of the nucleus (nucleokinesis (NK)) (Fig. 1.B). The neurons then pause and the cycle initiates again.

After an *in vivo* intraventricular electroporation of a GFP-expressing plasmid in neonate mice, a cohort of GFP-positive neurons can be visualized in the RMS a few days later (Fig. 1.C).

FMRP is expressed in most neurons of the Central Nervous System (CNS) (Gholizadeh *et al*, 2015). Accordingly, immunostaining for FMRP reveals that FMRP is strongly expressed in the RMS, where most neurons appear labeled. When observing individual GFP-positive neurons, FMRP labeling appears as a discrete and punctate

staining visible mainly in the cytoplasm both at the rear of the neuron and in the leading process and growth cone (Fig. 1.D,E).

The absence of FMRP leads to migration defects

To investigate the involvement of FMRP in RMS migration, we used the *Fmr1-null* mouse line (Fmr1 knockout mice: a model to study fragile X mental retardation. The Dutch-Belgian Fragile X Consortium, 1994). Time-lapse video microscopy of GFP positive neurons in the RMS shows major migratory impairments in *Fmr1-null* neurons as compared to controls (respectively movies S.1 and S.2). The position of each fluorescent neuron was tracked at each time point, generating x, y coordinates along its trajectory, thus enabling the quantification of various migration parameters. *Fmr1-null* neurons display a slowed-down migration, an increased pausing time, a more sinuous trajectory, and a defective directionality (Fig. 2.A-D). The nucleokinesis is less frequent in *Fmr1-null* neurons and the mean distance per NK is reduced (Fig. 2.E,F). The absence of FMRP thus leads to severe migratory defects.

The absence of FMRP impairs centrosomal dynamics

Given the crucial role of the centrosome in neuronal migration (Higginbotham & Gleeson, 2007), we analyzed its dynamics. We thus performed a co-electroporation of GFP and Centrine-RFP in *Fmr1-null* and control neonate mice to co-label migrating neurons and their centrosome (Fig. 3.A). A simultaneous tracking of the cell body and the centrosome enabled the quantification of centrosomal dynamics. The CK is slowed-down and less frequent in *Fmr1-null* neurons, as compared to control neurons (Fig. 3.B,C). To analyze the coordination of the centrosomal and the subsequent nuclear movement, we established a parameter quantifying CK efficiency. A CK leading to a subsequent NK was defined as an efficient CK as opposed to a CK not leading to an NK. CK efficiency is reduced in *Fmr1-null* neurons as compared to controls (Fig. 3.D), showing that the “two-stroke” cycle is compromised.
Taken together, these results show that FMRP plays a key role in neuronal migration.

***Fmr1* knockdown recapitulates migration defects of *Fmr1-null* neurons**

To assess whether these migration defects are cell autonomous, we designed an interfering RNA coupled to GFP to cell-autonomously knock-down *Fmr1* mRNA in RMS neurons, similar to (Scotto-Lomassese *et al*, 2011). The interfering miR*Fmr1*-GFP was co-injected with centrin-RFP in C57Bl6 neonate mice and time-lapse imaging was performed in acute sections of the RMS (movie S. 3). MiR*Fmr1*-GFP neurons migrate slowly, spend more time in pause, have a more sinuous and deviated trajectory, as compared to neurons expressing the miRNeg control plasmid (Fig. 4.A-D). MiR*Fmr1*-GFP neurons also exhibit NK defects (Fig. 4.E,F) and CK defects (Fig. 5.A-C). Overall statistical comparisons of GFP positive *Fmr1-null* neurons and miR*Fmr1*-GFP positive neurons show no significant difference for all migratory parameters. *Fmr1* KD is thus sufficient to recapitulate the entire migratory phenotype described in *Fmr1-null* neurons, showing that FMRP cell-autonomously regulates neuronal migration.

MAP1B expression is increased in *Fmr1-null* RMS neurons and *Map1b* KD rescues the migratory phenotype of *Fmr1-null* neurons

MAP1B is a neuron-specific microtubule-associated protein widely expressed in the developing CNS with crucial roles in diverse steps of neural development including neuronal migration (Yang *et al*, 2012). MAP1B is also a well-know FMRP mRNA target (Zhang *et al*, 2001)(Darnell *et al*, 2001)(Brown *et al*, 2001). It thus appeared as an interesting FMRP target to investigate.

As FMRP is a repressor of MAP1B mRNA translation (Brown *et al*, 2001)(Darnell *et al*, 2001)(Lu *et al*, 2004), the overall level of MAP1B usually appears increased in an *Fmr1-null* context (Lu *et al*, 2004)(Hou *et al*, 2006). Accordingly, immunostaining of MAP1B indeed showed its overexpression in the *Fmr1-null* RMS (Fig. S.1.A). Quantification of MAP1B expression by Western Blot of the RMS confirmed this increase (Fig. S.1.B).

To assess whether the upregulation of MAP1B is responsible for the migratory phenotype observed in *Fmr1-null* neurons, we designed an interfering RNA to cell-autonomously knock-down *Map1b* mRNA in RMS neurons. The miR*Map1b*-GFP, whose efficiency was assessed (Fig. S.2), was electroporated in *Fmr1-null* neonate mice and time-lapse imaging was performed in acute sections of the RMS (movie S. 4). *Fmr1-null* neurons expressing miR*Map1b*-GFP exhibit a completely restored migration speed, pausing time, NK distance and frequency, which become comparable

to miRNeg-GFP control neurons (Fig.6.A,B,D,E). Of note, the sinuosity of *Fmr1-null* neurons expressing miR*Map1b*-GFP was not rescued, staying similar as *Fmr1-null* neurons expressing the control miRNeg-GFP plasmid (Fig.6.C).
These results show that MAP1B is the main FMRP mRNA target involved in the regulation of neuronal migration.

DISCUSSION

FMRP is commonly described as a critical regulator of neuronal plasticity and neural development (Richter & Zhao, 2021). However, its role in neuronal migration remains poorly understood. We provide here clear evidence for its cell-autonomous role in postnatal migration and the causal role of its mRNA target MAP1B.

A role for FMRP in radial embryonic migration was evidenced by (La Fata *et al*, 2014) and (Wu *et al*, 2019). (La Fata *et al*, 2014) mainly analyzed defects in the multipolar to bipolar transition, which can be interpreted as a polarity defect rather than a migration defect *per se*. (Wu *et al*, 2019) reported neuronal misplacements after FMRP loss or gain of function in relation with MicroRNA-129 but did not analyze the dynamic of radial migration itself. To our knowledge, tangential migration in the absence of FMRP has never been analyzed so far, and neither has been the effect of its absence on the dynamic of saltatory migration, as analyzed by live-imaging like we did.
We report strong defects in postnatal migration with a slowed-down and erratic migration. Of importance, even though the mutated neurons are delayed in their movement and lose time finding the proper direction, they ultimately properly arrive in the OB, which we previously showed in the adult (Scotto-Lomassese *et al*, 2011). Live imaging allowed us to perform detailed analysis of both nucleokinesis and centrosome dynamics, which proved both to be deeply perturbed. As microtubules are essential regulators of both processes (Kuijpers & Hoogenraad, 2011) (Tsai & Gleeson, 2005), this led us to suspect MAP1B as the key FMRP mRNA target involved in the migratory phenotypes. MAP1B is one of the historic targets of FMRP (Brown *et al*, 2001)(Darnell *et al*, 2001)(Zhang *et al*, 2001). It is expressed early in the embryonic brain (Tucker *et al*, 1989) and is essential to different steps of neural development (Gonzalez-Billault *et al*, 2004). It is in particular involved in the reelin-dependent regulation of embryonic

radial migration (González-Billault *et al*, 2005), probably through its interaction with the LIS1-dynein complex (Jiménez-Mateos *et al*, 2005).
We show MAP1B overexpression in *Fmr1*-mutated neurons and rescue the migratory defects through its RNA-interference-induced KD. This identifies MAP1B as the critical FMRP mRNA target involved in the regulation of cyclic saltatory migration.
The importance of FMRP-regulated MAP1B translation was initially evidenced in *drosophila*, where it appeared essential for proper synaptogenesis (Zhang *et al*, 2001). This was later confirmed in the mouse hippocampus, where increased MAP1B levels in the *Fmr1*-null context also induced defective synaptogenesis, through increased microtubule stability (Lu *et al*, 2004). To our knowledge, the importance of the FMRP-MAP1B duo for neuronal migration that we report here is its only other described neurodevelopmental function. It would be important to assess whether our findings about the FMRP/MAP1B duo might extend to embryonic migration, as suggested by the combined importance of FMRP and of MAP1B in the final positioning of cortical glutamatergic neurons (Wu *et al*, 2019)(González-Billault *et al*, 2005).

Of note, the sinuosity of migrating neurons was not rescued by *Map1b* KD, suggesting that other FMRP mRNA targets might be involved in that process. FMRP has been associated with targets of the actomyosin pathway like cofilin and profilin (Michaelsen-Preusse *et al*, 2016)(Feuge *et al*, 2019), which are involved in growth cone motility and guidance (Omotade *et al*, 2017). Another possible target could be APC (Adenomatous Polyposis Coli), a recently described FMRP mRNA target (Maurin *et al*, 2018) also involved in the regulation of growth cone guidance (Koester *et al*, 2007).

In the context of FXS, analyzing tangential migration in the probably soon to be developed FXS human assembloïds will be of course of major interest (Levy & Paşca, 2023). It is to be noted that postnatal tangential migration in the infant human brain was recently described to be even more extensive than in mice (Paredes *et al*, 2016)(Sanai *et al*, 2011) so that, if conserved in humans, the defects that we observe might be critical for proper postnatal corticogenesis.

As a conclusion, we report here an entirely new function of FMRP as a regulator of migration linked to microtubules *via* MAP1B. This participates in the fundamental

understanding of this multifaceted protein and might also be important for the pathophysiological understanding of FXS.

FUNDINGS

This work was funded by Fondation Jérôme Lejeune, ANR NotifX ANR-20-CE16-0016 and NIH contract NIDCD Grant R01-DC-017989.

ACKNOWLEDGMENTS

We thank Isabelle Dusart for expert reading as well as Caroline Dubacq and Oriane Trouillard for technical help. The experiments were performed in IBPS imaging facility and the mice were housed in IBPS animal facility.

REFERENCES

Ascano M, Mukherjee N, Bandaru P, Miller JB, Nusbaum JD, Corcoran DL, Langlois C, Munschauer M, Dewell S, Hafner M, *et al* (2012) FMRP targets distinct mRNA sequence elements to regulate protein expression. *Nature* 492: 382–386

Banerjee A, Ifrim MF, Valdez AN, Raj N & Bassell GJ (2018) Aberrant RNA translation in fragile X syndrome: From FMRP mechanisms to emerging therapeutic strategies. *Brain Res* 1693: 24–36

Bellion A, Baudoin J-P, Alvarez C, Bornens M & Métin C (2005) Nucleokinesis in Tangentially Migrating Neurons Comprises Two Alternating Phases: Forward Migration of the Golgi/Centrosome Associated with Centrosome Splitting and Myosin Contraction at the Rear. *J Neurosci* 25: 5691–5699

Brown V, Jin P, Ceman S, Darnell JC, O'Donnell WT, Tenenbaum SA, Jin X, Feng Y, Wilkinson KD, Keene JD, *et al* (2001) Microarray Identification of FMRP-Associated Brain mRNAs and Altered mRNA Translational Profiles in Fragile X Syndrome. *Cell* 107: 477–487

Darnell JC, Jensen KB, Jin P, Brown V, Warren ST & Darnell RB (2001) Fragile X Mental Retardation Protein Targets G Quartet mRNAs Important for Neuronal Function. *Cell* 107: 489–499

Daroles L, Gribaudo S, Doulazmi M, Scotto-Lomassese S, Dubacq C, Mandairon N, Greer CA, Didier A, Trembleau A & Caillé I (2016) Fragile X Mental Retardation Protein and Dendritic Local Translation of the Alpha Subunit of the Calcium/Calmodulin-Dependent Kinase II Messenger RNA Are Required for the Structural Plasticity Underlying Olfactory Learning. *Biol Psychiatry* 80: 149–159

Davis JK & Broadie K (2017) Multifarious Functions of the Fragile X Mental Retardation Protein. *Trends Genet* 33: 703–714

Feuge J, Scharkowski F, Michaelsen-Preusse K & Korte M (2019) FMRP Modulates Activity-Dependent Spine Plasticity by Binding Cofilin1 mRNA and Regulating Localization and Local Translation. *Cereb Cortex* 29: 5204–5216

Fmr1 knockout mice: a model to study fragile X mental retardation. The Dutch-Belgian Fragile X Consortium (1994) *Cell* 78: 23–33

Gholizadeh S, Halder SK & Hampson DR (2015) Expression of fragile X mental retardation protein in neurons and glia of the developing and adult mouse brain. *Brain Res* 1596: 22–30

González-Billault C, Del Río JA, Ureña JM, Jiménez-Mateos EM, Barallobre MJ, Pascual M, Pujadas L, Simó S, Torre AL, Gavin R, *et al* (2005) A role of MAP1B in Reelin-dependent neuronal migration. *Cereb Cortex N Y N 1991* 15: 1134–1145

Gonzalez-Billault C, Jimenez-Mateos EM, Caceres A, Diaz-Nido J, Wandosell F & Avila J (2004) Microtubule-associated protein 1B function during normal development, regeneration, and pathological conditions in the nervous system. *J Neurobiol* 58: 48–59

Higginbotham HR & Gleeson JG (2007) The centrosome in neuronal development. *Trends Neurosci* 30: 276–283

Hou L, Antion MD, Hu D, Spencer CM, Paylor R & Klann E (2006) Dynamic translational and proteasomal regulation of fragile X mental retardation protein controls mGluR-dependent long-term depression. *Neuron* 51: 441–454

Jiménez-Mateos EM, Wandosell F, Reiner O, Avila J & González-Billault C (2005) Binding of microtubule-associated protein 1B to LIS1 affects the interaction between dynein and LIS1. *Biochem J* 389: 333–341

Koester MP, Müller O & Pollerberg GE (2007) Adenomatous Polyposis Coli Is Differentially Distributed in Growth Cones and Modulates Their Steering. *J Neurosci* 27: 12590–12600

Kuijpers M & Hoogenraad CC (2011) Centrosomes, microtubules and neuronal development. *Mol Cell Neurosci* 48: 349–358

La Fata G, Gärtner A, Domínguez-Iturza N, Dresselaers T, Dawitz J, Poorthuis RB, Averna M, Himmelreich U, Meredith RM, Achsel T, *et al* (2014) FMRP regulates multipolar to bipolar transition affecting neuronal migration and cortical circuitry. *Nat Neurosci* 17: 1693–1700

Levy RJ & Paşca SP (2023) What Have Organoids and Assembloids Taught Us About the Pathophysiology of Neuropsychiatric Disorders? *Biol Psychiatry* 93: 632–641

Lim DA & Alvarez-Buylla A (2016) The Adult Ventricular–Subventricular Zone (V-SVZ) and Olfactory Bulb (OB) Neurogenesis. *Cold Spring Harb Perspect Biol* 8: a018820

Lois C, García-Verdugo JM & Alvarez-Buylla A (1996) Chain migration of neuronal precursors. *Science* 271: 978–981

Lu R, Wang H, Liang Z, Ku L, O'donnell WT, Li W, Warren ST & Feng Y (2004) The fragile X protein controls microtubule-associated protein 1B translation and microtubule stability in brain neuron development. *Proc Natl Acad Sci U S A* 101: 15201–15206

Maurin T, Lebrigand K, Castagnola S, Paquet A, Jarjat M, Popa A, Grossi M, Rage F & Bardoni B (2018) HITS-CLIP in various brain areas reveals new targets and new modalities of RNA binding by fragile X mental retardation protein. *Nucleic Acids Res* 46: 6344–6355

Michaelsen-Preusse K, Zessin S, Grigoryan G, Scharkowski F, Feuge J, Remus A & Korte M (2016) Neuronal profilins in health and disease: Relevance for spine plasticity and Fragile X syndrome. *Proc Natl Acad Sci* 113: 3365–3370

Moro F, Pisano T, Bernardina BD, Polli R, Murgia A, Zoccante L, Darra F, Battaglia A, Pramparo T, Zuffardi O, *et al* (2006) Periventricular heterotopia in fragile X syndrome. *Neurology* 67: 713–715

Omotade OF, Pollitt SL & Zheng JQ (2017) Actin-based growth cone motility and guidance. *Mol Cell Neurosci* 84: 4–10

Paredes MF, James D, Gil-Perotin S, Kim H, Cotter JA, Ng C, Sandoval K, Rowitch DH, Xu D, McQuillen PS, *et al* (2016) Extensive migration of young neurons into the infant human frontal lobe. *Science* 354: aaf7073

Richter JD & Zhao X (2021) The molecular biology of FMRP: new insights into fragile X syndrome. *Nat Rev Neurosci* 22: 209–222

Romero DM, Bahi-Buisson N & Francis F (2018) Genetics and mechanisms leading to human cortical malformations. *Semin Cell Dev Biol* 76: 33–75

Sanai N, Nguyen T, Ihrie RA, Mirzadeh Z, Tsai H-H, Wong M, Gupta N, Berger MS, Huang E, Garcia-Verdugo J-M, *et al* (2011) Corridors of migrating neurons in the human brain and their decline during infancy. *Nature* 478: 382–386

Scotto-Lomassese S, Nissant A, Mota T, Néant-Féry M, Oostra BA, Greer CA, Lledo P-M, Trembleau A & Caillé I (2011) Fragile X Mental Retardation Protein Regulates New Neuron Differentiation in the Adult Olfactory Bulb. *J Neurosci* 31: 2205–2215

Stoufflet J, Chaulet M, Doulazmi M, Fouquet C, Dubacq C, Métin C, Schneider-Maunoury S, Trembleau A, Vincent P & Caillé I (2020) Primary cilium-dependent cAMP/PKA signaling at the centrosome regulates neuronal migration. *Sci Adv* 6: eaba3992

Tsai L-H & Gleeson JG (2005) Nucleokinesis in Neuronal Migration. *Neuron* 46: 383–388

Tucker RP, Garner CC & Matus A (1989) In situ localization of microtubule-associated protein mRNA in the developing and adult rat brain. *Neuron* 2: 1245–1256

Wu C, Zhang X, Chen P, Ruan X, Liu W, Li Y, Sun C, Hou L, Yin B, Qiang B, *et al* (2019) MicroRNA-129 modulates neuronal migration by targeting Fmr1 in the developing mouse cortex. *Cell Death Dis* 10: 1–13

Yang M, Wu M, Xia P, Wang C, Yan P, Gao Q, Liu J, Wang H, Duan X & Yang X (2012) The role of microtubule-associated protein 1B in axonal growth and neuronal migration in the central nervous system. *Neural Regen Res* 7: 842–848

Zhang YQ, Bailey AM, Matthies HJG, Renden RB, Smith MA, Speese SD, Rubin GM & Broadie K (2001) Drosophila Fragile X-Related Gene Regulates the MAP1B Homolog Futsch to Control Synaptic Structure and Function. *Cell* 107: 591–603

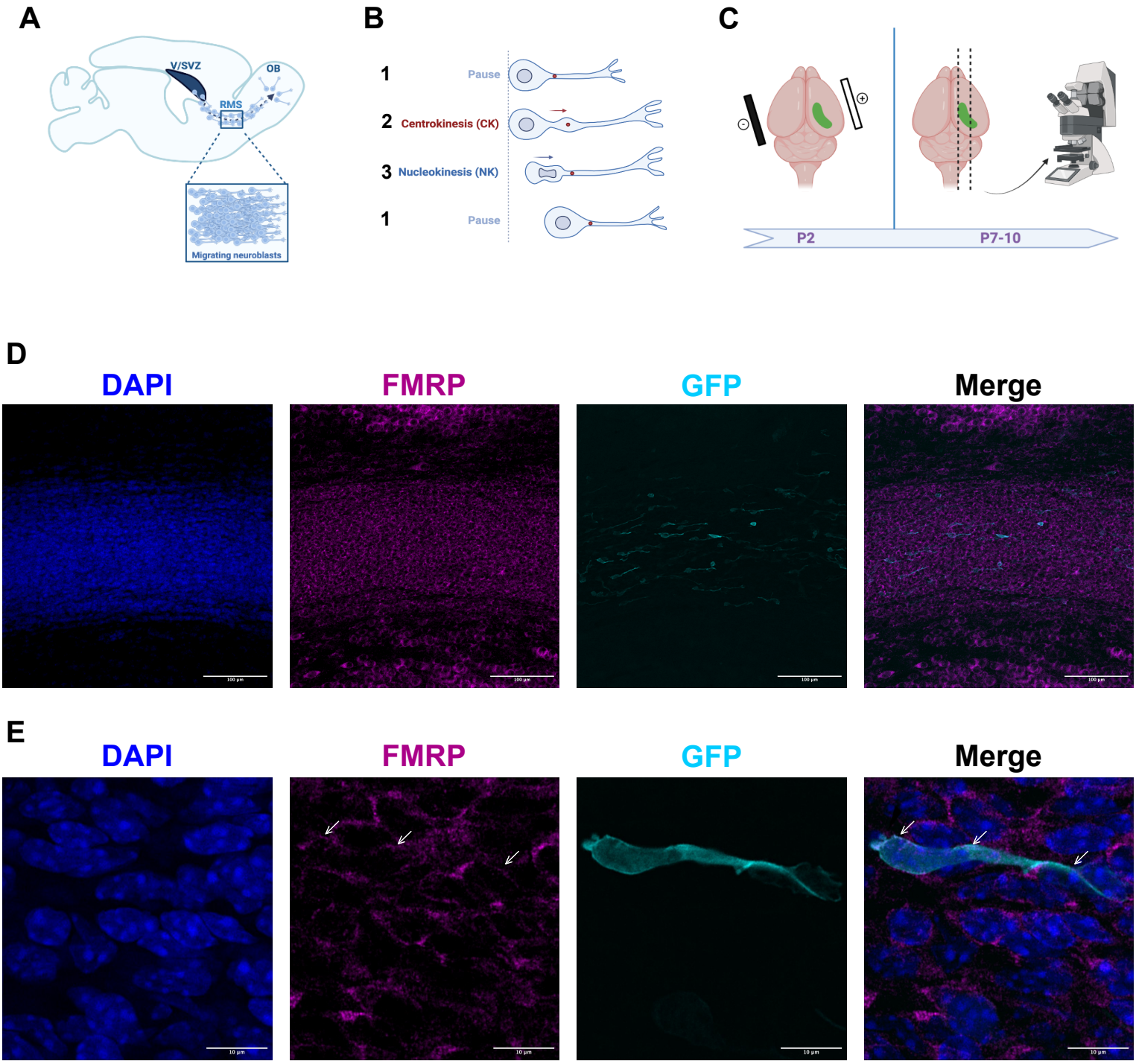

FIGURE 1. ***FMRP is expressed in migrating neurons of the murine postnatal RMS.*** *(A) Scheme of a sagittal section of the postnatal RMS connecting the V/SVZ to the OB. V/SVZ, ventricular/sub-ventricular zone; OB, olfactory bulb; RMS, rostral migratory stream. The inset shows the high density of homotypically migrating neurons in the RMS. (B) Representation of neuroblasts' cyclic saltatory migration. 1. The neuron is in pause. 2. The leading process (LP) extends, and the centrosome moves within a swelling in the LP. 3. The nucleus moves forward. CK, centrokinesis; NK, nucleokinesis. (C) Scheme of the experimental procedure. 2-day old neonates are intraventricularly electroporated with a GFP-expressing plasmid to label a cohort of migrating neurons that can be subsequently visualized in fixed or acute sections of the RMS. (D) Immunohistochemistry of the RMS showing FMRP expression (magenta) along the stream, in which a cohort of GFP-positive neurons (cyan) are visible. Scale bar: 100 µm. (E) Immunohistochemistry of a GFP-positive RMS neuron (cyan) showing FMRP subcellular expression (magenta). The GFP-positive neuron displays a cytoplasmic expression of FMRP around the nucleus (indicated by white arrows), along the leading process and in the growth cone. The surrounding GFP-negative neurons express FMRP as well, according to the same pattern. Scale bar: 10 µm.*

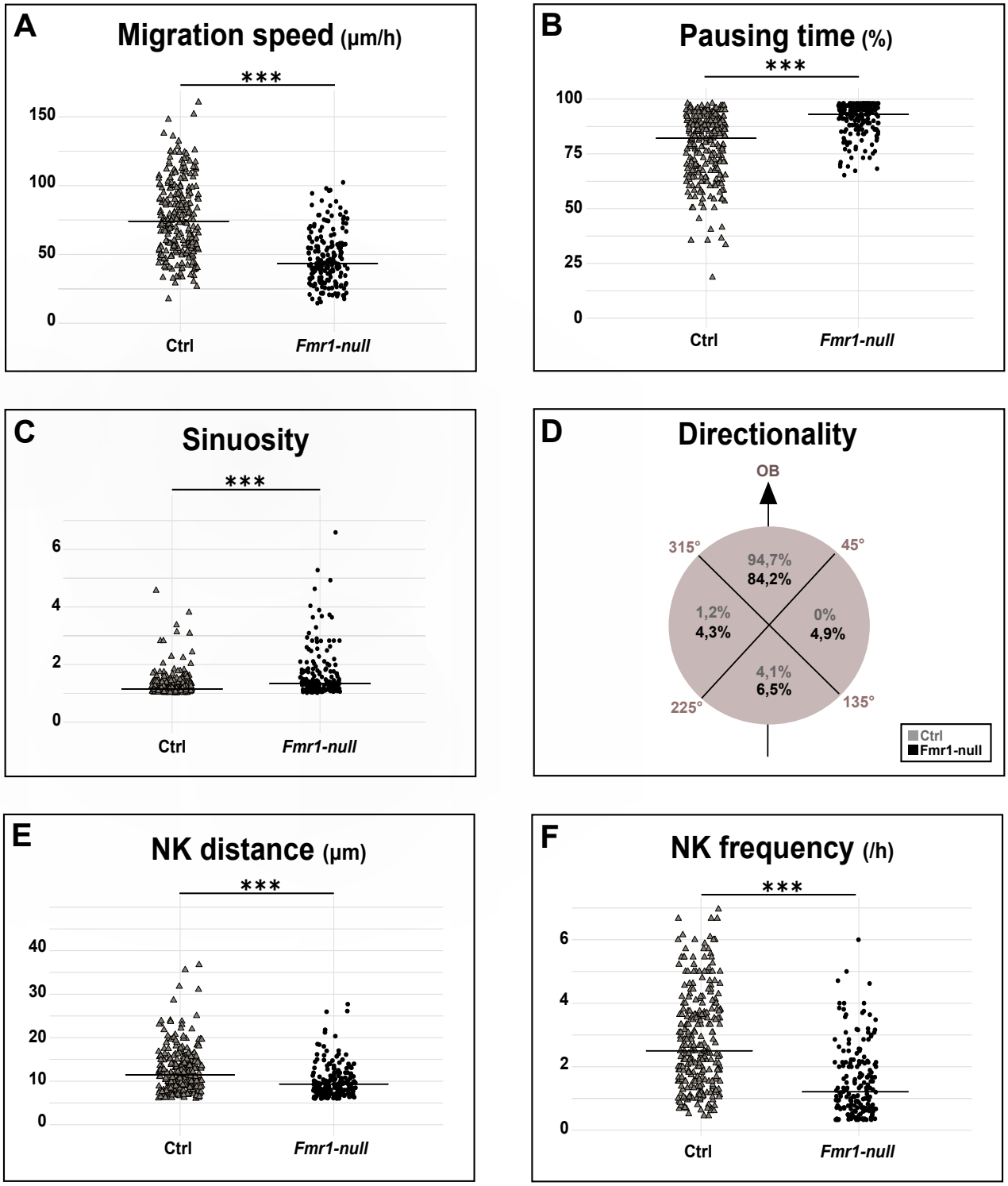

FIGURE 2. ***Migration defects in Fmr1-null neurons.*** *(A) Migration speed of control (Ctrl) and Fmr1-null neurons. Ctrl: 76 ± 2 µm/h; Fmr1-null: 47 ± 1 µm/h (Mann-Whitney test, p-value < 0.001). (B) Percentage of pausing time of control and Fmr1-null neurons. Ctrl: 78 %; Fmr1-null: 91 % (Mann-Whitney test, p-value < 0.001). (C) Sinuosity index of control and Fmr1-null neurons. Ctrl: 1.32 ± 0.04; Fmr1-null: 1.93 ± 0.16 (Mann-Whitney test, p-value < 0.001). (D) Migration directionality radar represented in four spatial dials. Percentage of cells migrating in each spatial direction in control and Fmr1-null neurons, relatively to the vector going straight from the SVZ to the OB. (Fisher's Exact test, p-value < 0.001). (E) NK mean distance of control and Fmr1-null neurons. Ctrl: 12.5 ± 0.3 µm; Fmr1-null: 10.9 ± 0.8 µm (Mann-Whitney test, p-value < 0.001). (F) NK frequency of control and Fmr1-null neurons. Ctrl: 2.9 ± 0.1 NK/h; Fmr1-null: 1.5 ± 0.1 NK/h (Mann-Whitney test, p-value < 0.001). The black line represents the median. Ctrl: N = 3, n = 275; Fmr1-null: N = 3, n = 184. ***p-value < 0.001.*

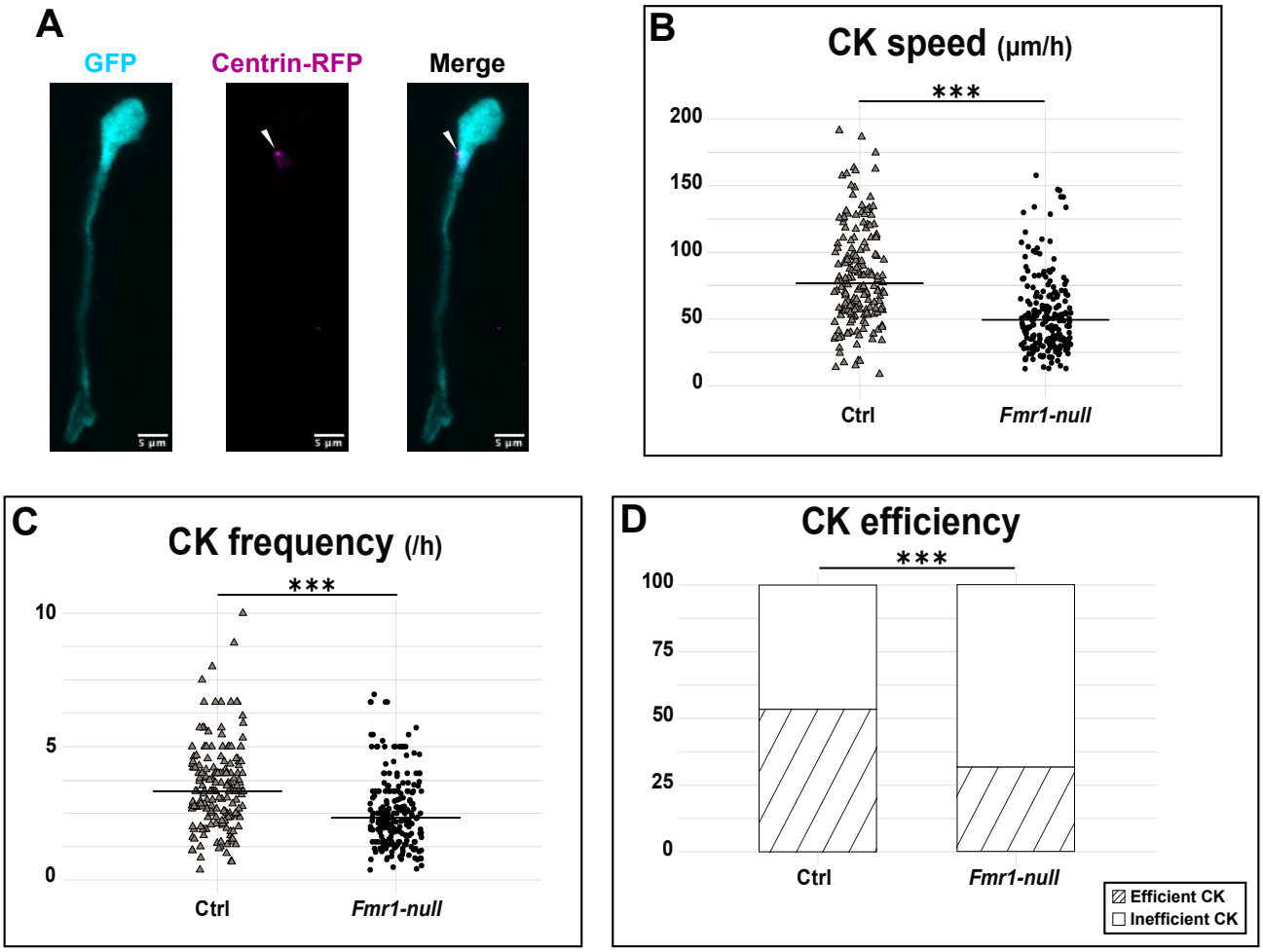

FIGURE 3. *CK defects in Fmr1-null neurons.* *(A) Illustration of an RMS-migrating neuron (cyan) co-injected with centrin-RFP (magenta). Scale bar: 5 µm. (B) CK speed of control and Fmr1-null neurons. Ctrl: 82 ± 3 µm/h; Fmr1-null: 54 ± 2 µm/h (Mann-Whitney test, p-value < 0.001). (C) CK frequency of control and Fmr1-null neurons. Ctrl: 3.5 ± 0.1 CK/h; Fmr1-null: 2.6 ± 0.1 CK/h (Mann-Whitney test, p-value < 0.001). (D) Percentage of efficient CKs in control and Fmr1-null neurons. Ctrl: 54 %; Fmr1-null: 33 % (Chi2 = 57.611, p-value < 0.001). The black line represents the median. Ctrl: N = 3, n = 178; Fmr1-null: N = 3, n = 216. *** p-value < 0.001.*

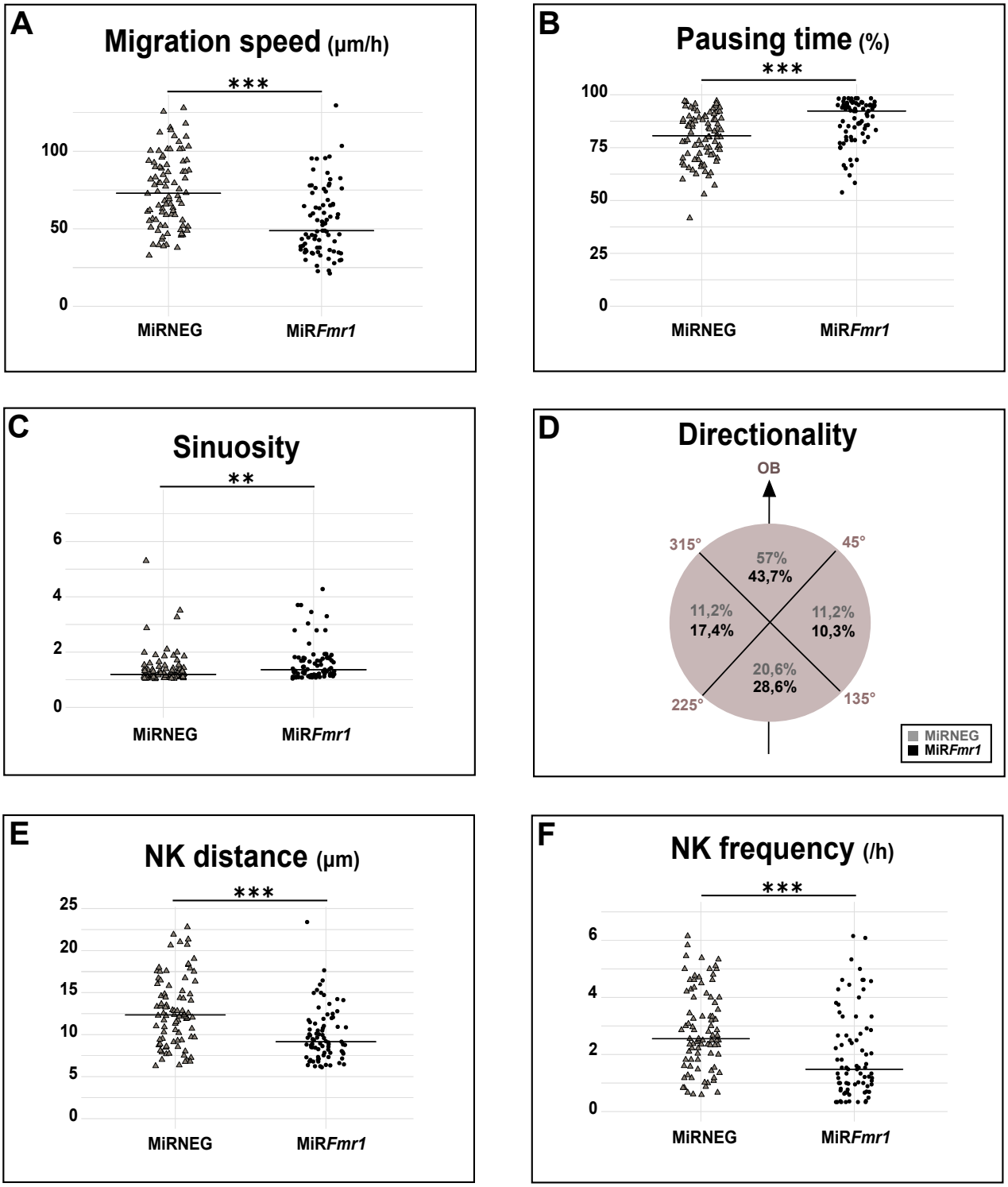

FIGURE 4. *Fmr1 KD recapitulates Fmr1-null neuronal migration defects.* *(A) Migration speed of neurons expressing MiRNEG and MiRFmr1. MiRNEG: 75 ± 3 µm/h; MiRFmr1: 55 ± 2 µm/h (Mann-Whitney test, p-value < 0.001). (B) Percentage of pausing time of neurons expressing MiRNEG and MiRFmr1. MiRNEG: 80 %; MiRFmr1: 88 % (Mann-Whitney test, p-value < 0.001). (C) Sinuosity index of neurons expressing MiRNEG and MiRFmr1. MiRNEG: 1.50 ± 0.12; MiRFmr1: 1.62 ± 0.08 (Mann-Whitney test, p-value = 0.003). (D) Migration directionality radar represented in four spatial dials. Percentage of cells migrating in each spatial direction in neurons expressing MiRNEG and MiRFmr1, relatively to the vector going straight from the SVZ to the OB. (Fisher's Exact test, p-value = 0.019). (E) NK mean distance of neurons expressing MiRNEG and MiRFmr1. MiRNEG: 12.8 ± 0.4 µm; MiRFmr1: 9.9 ± 0.4 µm (Mann-Whitney test, p-value < 0.001). (F) NK frequency of neurons expressing MiRNEG and MiRFmr1. MiRNEG: 2.9 ± 0.2 NK/h; MiRFmr1: 2.0 ± 0.2 NK/h (Mann-Whitney test, p-value < 0.001). The black line represents the median. MiRNEG: N = 3, n = 86; MiRFmr1: N = 3, n = 79. * p-value < 0.05; ** p-value < 0.005; *** p-value < 0.001.*

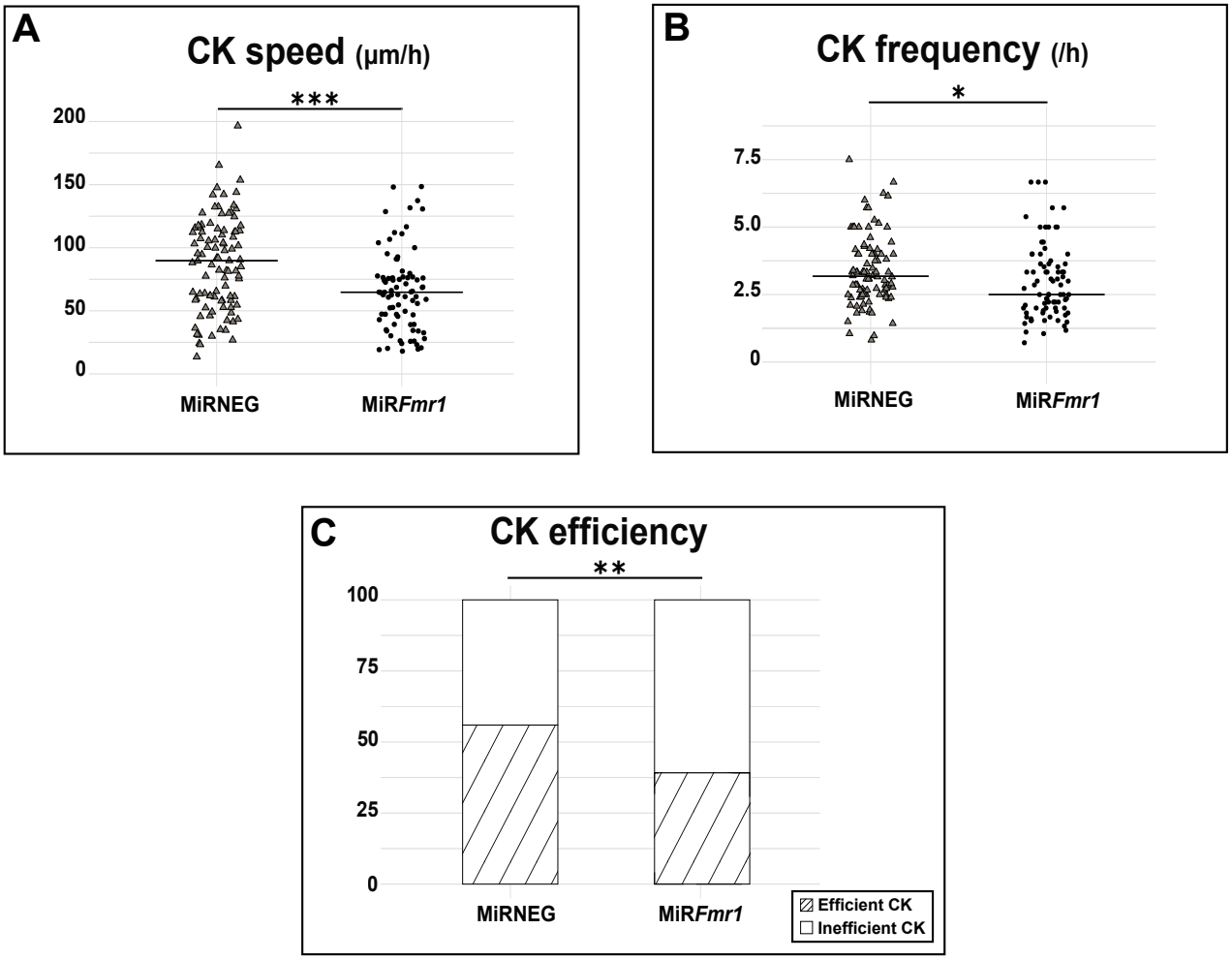

FIGURE 5. ***Fmr1 KD recapitulates Fmr1-null neurons CK defects.*** *(A) CK speed of neurons expressing MiRNEG and MiRFmr1. MiRNEG: 87 ± 4 µm/h; MiRFmr1: 66 ± 3 µm/h (Mann-Whitney test, p-value < 0.001). (B) CK frequency of neurons expressing MiRNEG and MiRFmr1. MiRNEG: 3.4 ± 0.1 CK/h; MiRFmr1: 3.0 ± 0.2 CK/h (Mann-Whitney test, p-value = 0.011). (C) Percentage of efficient CKs in neurons expressing MiRNEG and MiRFmr1. MiRNEG: 57 %; MiRFmr1: 41 % (Chi2 = 17.999, p-value = 0.0012). The black line represents the median. MiRNEG: N = 3, n = 96; MiRFmr1: N = 3, n = 81. *p-value < 0.05; **p-value < 0.005; *** p-value < 0.001.*

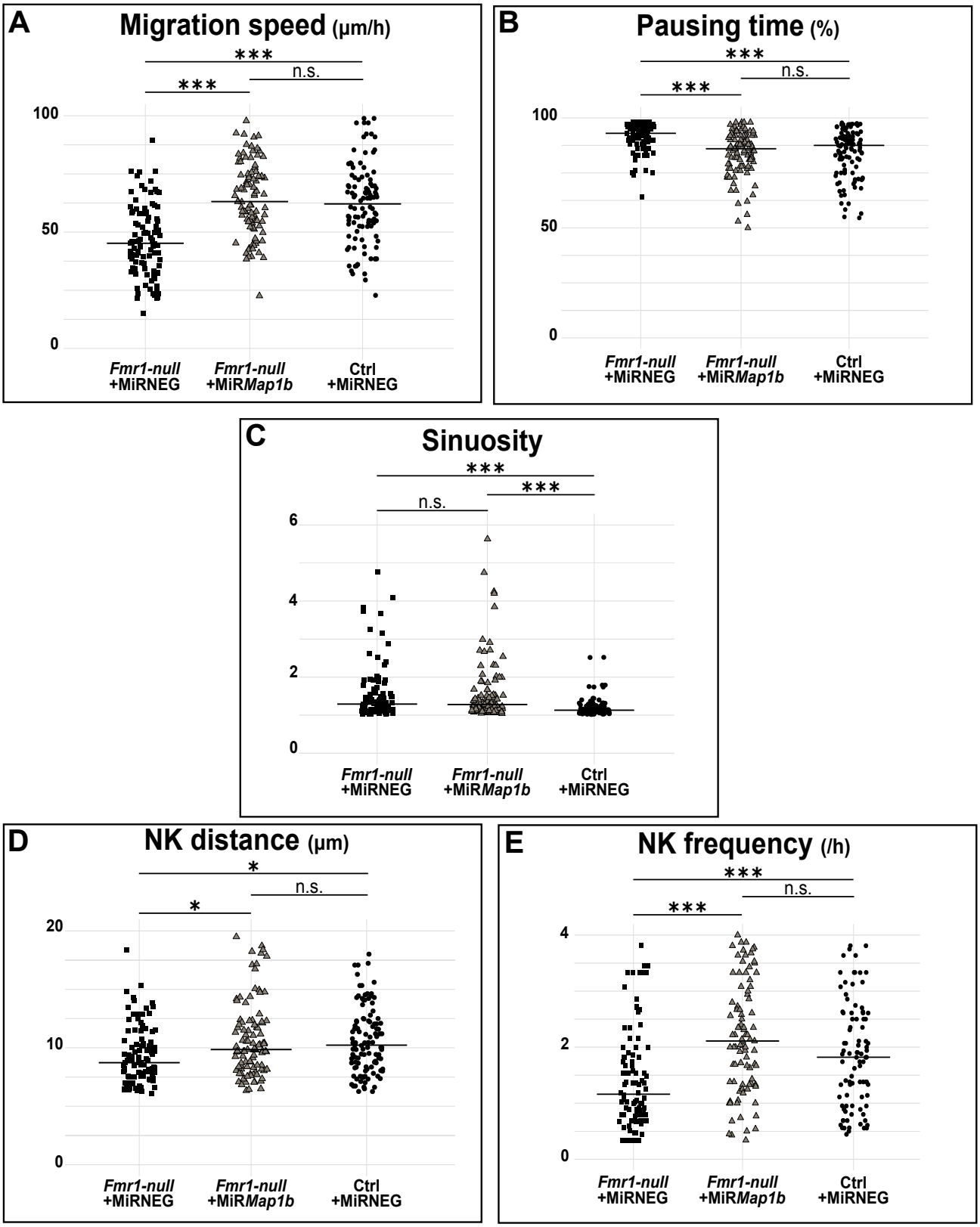

FIGURE 7. *Map1b KD rescues Fmr1-null neurons migration defects.* *(A) Migration speed of Fmr1-null neurons expressing MiRNEG and MiRMap1b and control neurons expressing MiRNEG. Fmr1-null neurons + MiRNEG: 47 ± 2 µm/h; Fmr1-null neurons + MiRMap1b: 67 ± 2 µm/h; control neurons + MiRNEG: 64 ± 2 µm/h (Kruskall-Wallis Test: Chi2 = 61.168, p-value < 0.001, df = 2; followed by Dunn's posthoc test). (B) Percentage of pausing time of Fmr1-null neurons expressing MiRNEG and MiRMap1b and control neurons expressing MiRNEG. Fmr1-null neurons + MiRNEG: 92 %; Fmr1-null neurons + MiRMap1b: 84 %; control neurons + MiRNEG: 84 % (Kruskall-Wallis Test: Chi2 = 45.716, p-value < 0.001, df = 2; followed by Dunn's posthoc test). (C) Sinuosity index of Fmr1-null neurons expressing MiRNEG and MiRMap1b and control neurons expressing MiRNEG. Fmr1-null neurons + MiRNEG: 1.77 ± 0.18; Fmr1-null neurons + MiRMap1b: 1.90 ± 0.20; control neurons + MiRNEG: 1.18 ± 0.02 (Kruskall-Wallis Test: Chi2 = 39.807, p-value < 0.001, df = 2; followed by Dunn's posthoc test). (D) NK mean distance of Fmr1-null neurons expressing MiRNEG and MiRMap1b and control neurons expressing MiRNEG. Fmr1-null neurons + MiRNEG: 9.7 ± 0.3 µm; Fmr1-null neurons + MiRMap1b: 11.1 ± 0.4 µm; control neurons + MiRNEG: 10.6 ± 0.3 µm (Kruskall-Wallis Test: Chi2 = 11.573, p-value = 0.003, df = 2; followed by Dunn's posthoc test). (E) NK frequency of Fmr1-null neurons expressing MiRNEG and MiRMap1b and control neurons expressing MiRNEG. Fmr1-null neurons + MiRNEG: 1.5 ± 0.1 NK/h; Fmr1-null neurons + MiRMap1b: 2.4 ± 0.1 NK/h; control neurons + MiRNEG: 2.5 ± 0.2 NK/h (Kruskall-Wallis Test: Chi2 = 39.272, p-value < 0.001, df = 2; followed by Dunn's posthoc test). The black line represents the median. Fmr1-null neurons + MiRNEG: N = 6, n = 102; Fmr1-null neurons + MiRMap1b: N = 3, n = 101; control neurons + MiRNEG: N = 3, n = 78. * p-value < 0.05; *** p-value < 0.001; n.s. (not significant), p-value > 0.05.*